JOURNAL OF SPACECRAFT AND ROCKETS
Vol. 37, No. 3, May–June 2000

Modeling the Outer Belt Enhancements of Penetrating Electrons

Gordon L. Wrenn* and David J. Rodgers†
Defence Evaluation and Research Agency, Farnborough, Hampshire, England GU14 0LX, United Kingdom
and
Paul Buehler‡
Paul Scherrer Institute, CH-5232 Villigen PSI, Switzerland

Mega-electron volt electrons in the outer radiation belt present a spacecraft hazard in the form of internal charging effects during periods of flux enhancement that often result from the interaction of high-speed solar wind streams with the Earth's magnetosphere. The morphology of these enhancements throughout a complete solar cycle is described using data from spacecraft in geosynchronous and geostationary-transfer orbits; this then permits the development of an empirical flux model for an engineering software tool designed to assess the vulnerability of satellite systems to the electrostatic charging of shielded dielectrics. This model, named FLUMIC, is unrefined but has a specific focus to serve a practical need and is very simple to use; it also represents one step in a universal quest to pension off the venerated but largely inadequate AE-8 code.

Nomenclature

$a(L)$ = flux scaling factor
$b(L)$ = energy scaling factor
E = energy, MeV
E_R = reference energy, 2 MeV
E_0 = e-folding energy, MeV
F_E = integral flux with energy $> E$, cm^{-2} day^{-1} sr^{-1}
F_R = integral flux $> E_R$, cm^{-2} day^{-1} sr^{-1}
L = McIlwain parameter, R_e

Introduction

VERY energetic electrons in the outer magnetosphere are trapped or pseudotrapped in a magnetic field that is dominated by the Earth's dipole but is often significantly perturbed by dynamic interactions of the solar wind and the large current flows that these induce. Persistent two or three orders of magnitude flux intensifications of these electrons, with energy in the range of 0.1–10 MeV, occur regularly. Such electrons can penetrate spacecraft surface structures and deposit charge within dielectric materials; the subsequent electrostatic discharges represent a real hazard for high-altitude satellites.[1,2]

The engineering requirement to assess the vulnerability of spacecraft components to internal charging has now been addressed by the development of an engineering software tool (DICTAT).[3] To predict the highest fluences of penetrating electrons to be expected during any mission, it is necessary to have an appropriate model of the outer belt and the flux model for internal charging (FLUMIC) has been constructed to this end.

Problem

AE-8 (Ref. 4) has been universally used since 1983 to describe the energetic electron environment, but it is a static average model that has long been recognized as seriously inadequate in the outer zone and just an extrapolation of unknown validity above 2 MeV (Ref. 5). The outer belt encompasses two distinct components that have different origins and motions, giving rise to contrasting spatial and temporal variations. Cayton et al.[6] quantitatively described these components observed at geosynchronous orbit (GEO) as soft (30–300 keV with $T_s \sim 25$ keV) and hard (300–2000 keV with $T_h \sim 200$ keV). The soft electrons are part of the plasmasheet energized in transient substorm injections; they appear on auroral field lines, reflecting a nightside bias and a close link to geomagnetic activity indices. The hard component tends to be more stably trapped, but nevertheless it regularly undergoes huge flux enhancements, often occurring periodically and persisting for many days. Whereas the soft population tends to dominate near solar maximum, the hard population exhibits peak intensities during the declining phase approaching solar minimum. It is not meaningful to integrate the two components to afford any typical spectrum or average fluence, and a more focused model than AE-8 is required.

The strength of the induced internal electric field depends on the rates of charge deposition and leakage; the characteristic charging time relates to the permittivity and conductivity of the dielectric material involved. The importance of this time in relation to the rate of change of electron flux, due to either the motion of the satellite through the magnetosphere or the temporal variability of the outer belt population, is its constraint on the data selection and averaging procedures for calculating an appropriate model. The maximum electric field strength is inversely proportional to conductivity, as is the charging time constant. Given the finite current density in the outer belt, this means that critical internal charging is restricted to dielectrics of very low conductivity, and it also requires prolonged exposures. The requirement is to characterize worst-case environments to assess the maximum level of internal charging for any particular spacecraft configuration and geometry. Worst-case presupposes high fluence, but the depth profile of charge deposition depends on shielding thickness and the incident energy spectrum, making it site specific. The harder the spectrum then the more penetrating are many of the electrons, but this does not necessarily produce a higher E field in the susceptible dielectric. Because instruments for the detection of mega-electron volt (MeV) electrons are not easily constructed, they have not been widely deployed; accurate calibration is particularly difficult. There are then a number of specific but interdependent aspects to be considered in establishing the modeling methodology.

Orbital location, L Value

Where electrostatic discharge (ESD) effects have been reported as due to internal charging, they have invariably occurred in the outer radiation belt, and it is reasonable to assume that penetrating electrons with fluences sufficient to cause ESDs are confined to magnetic field lines that map to high altitudes, that is, greater than about $3R_e$. For modeling purposes, the McIlwain L value provides a simple ordering of the data; the outer belt can then be portrayed as extending between $L = 3$ and $L = 8$, with the peak flux of penetrating electrons being encountered between $L = 4$ and $L = 5$.

The GEO has special interest because of the large number of platforms and the reduced range of dependent variables; it permits

Received 11 February 1999; revision received 15 December 1999; accepted for publication 10 January 2000.

*Consultant, Space Department; currently at TS Space Systems, 33-MJC, Hampshire, England RG29 1AP, United Kingdom.
†Senior Scientist, Space Department.
‡Research Scientist, Laboratory for Astrophysics.

almost continuous sampling of outer belt electrons even though it is well outside the peak fluxes, and important conclusions can be obtained from studies of such measurements. GEO spacecraft positioned on the geomagnetic equator lie near $L = 6.6$, but others see a diurnal variation in L with nightside values sometimes reaching 7.5, due to field asymmetry and tail distortion. The geotransfer orbit (GTO) is also important because it provides the opportunity to measure in just a few hours a near-equatorial radial profile in L.

Tying measurements to L value requires a reliable magnetic field model and can be accomplished out to $L = 8$ in geomagnetically quiet times. Although activity-dependent field models now exist,[7] it is very difficult to integrate data properly from disturbed periods. The best approach is to use L values that correspond with a quiet-time assumption and to neglect flux measurements obtained when K_p is large, for example, >3+. This is less questionable than it might appear because outer belt electron enhancements (OBEEs) tend to peak a few days after storm events, when the field has returned to a relatively stable configuration.

Appropriate Timescale

Operational anomalies reported to be effects of internal charging on GEO communications satellites coincide with the enhancements but typically require charging times between one and three days.[8] The notable failures of the Anik E1 and E2 satellites in 1994 have actually been rationalized in terms of a 9-day charge accumulation.[9] Spacecraft passing through the peak of the outer belt encounter higher fluxes, but invariably this is only for a small fraction of each orbit. FLUMIC is concerned with the high extremes of fluence to be expected during a mission and is, therefore, based on peak values of orbit integrations of the fluxes, daily fluences in GEO, rather than transient highs or long-term averages.

Low Energy Cutoff

Logically a cutoff should be defined by the desire to discriminate between surface and internal charging processes, but physically there is actually no sharp boundary. Instead, the reality of the two-component population suggests a cutoff that prevents significant contamination of flux integrations from the softer plasmasheet electrons. Spacecraft Environment Monitor-2 (SEM-2) detectors on METEOSAT-3 in GEO sampled electrons between 43 and 300 keV, and a detailed analysis of these data has been undertaken.[10] During OBEEs, the 06 h to 18 h LT fluence for the 200–300-keV channel was greater than that for 18 h to 06 h LT, in contrast to the lower energy channels. This simple test serves to discriminate between hard and soft, and it is concluded that 200 keV is appropriate for the required cutoff. The range of 200-keV electrons in aluminum is approximately 0.16 mm, but the flux cutoff does not preclude any calculation of total charge deposition being extrapolated to lower thicknesses.

Study of surface charging also requires a detailed knowledge of secondary and photoemission, but simulation codes such as NASCAP[11] have been used with much success. The existence of surface charge may well influence the evolution of internal electric fields, but given their much shorter timescales, these processes can be treated, to a first approximation, as an effective grounding of the exposed surface.

Available Data and Models

The radiation belts were much explored in the 1960s and 1970s, and data from that era were skillfully consolidated into empirical models such as AE-8. However, the limitations of the latter have been clearly exposed, and a model designed for this application has contrasting requirements: 1) a bias toward electrons with energy > 1 MeV; 2) a bias toward measurements at high equatorial altitudes, $L > 3$; 3) restriction to periods of enhanced flux; 4) calculation of peak fluence with integration matched to timescale of the internal charging process; 5) proper accounting of seasonal and solar cycle variations; and 6) a basic representation of spectral hardness.

Empirical models need good measurements, but during the last couple of decades few radiation belt data have been gathered. Improved detectors of MeV electrons have been developed but mainly flown in or near GEO, for example, using geostationary operational environment satellites (GOES), Los Alamos National Laboratory (LANL) energetic spectrometer for particles (ESP) instruments[12] on numerous spacecraft, SCATHA, and METEOSAT-3.[9] More recent results from HIPPARCOS,[13] CRRES,[14] and STRV-1[15] in GTO together with observations at low altitude from SAMPEX[16] have expanded the picture of outer belt dynamics.

Outer Belt Enhancements

High-Speed Solar Wind Streams

An inadequacy of AE-8 stems from the consequence of time averaging a variable flux that continually exhibits a series of discrete enhancements, although it is only these enhancements of the outer belt electrons that produce a risk of internal ESD. For an empirical model, it is not necessary to understand the physical processes that control the fluxes, but it is essential to establish the associated time constants. Figure 1 shows the pattern for typical daily fluence enhancements of >2-MeV electrons seen by GOES-7 in January/February 1995. Increases of between 2 and 3 orders of magnitude occur over a few days and are maintained for up to 10 days.

Measurements of daily mean solar wind speed from the WIND spacecraft near the L1 point are also plotted, and the relationship is clear; the majority of enhancements are observed to follow promptly the arrival of high-speed streams at the Earth. Such streams also undoubtedly cause geomagnetic storms, and a partial correlation between maximum electron flux and minimum *Dst* has been demonstrated.[17] The streams carry the interplanetary magnetic field (IMF) and its direction controls their interaction with the magnetosphere; the more intense OBEEs appear to correspond with southward IMF.

Recurrent and Nonrecurrent Enhancements: Solar Triggers

High-speed streams are associated with coronal holes appearing on the solar disk. These coronal holes often persist for a number of solar rotations and in consequence OBEEs tend to recur after about 27 days; therefore, it is logical to use 27.4 day Carrington rotations (CRs) to order data for monitoring these temporal variations. The 27-day recurrence is often clear, but the actuality or visibility of such recurrence depends on the frequency and stability of the high-speed streams, which both vary throughout the solar cycle with a degree of predictability. However, a number of nonrecurrent enhancements have occurred in association with solar proton events (SPEs) and coronal mass ejections (CMEs). The SPEs of March 1991 and May 1992 are very good examples of some extreme events when it has been possible to measure electron fluxes in the presence of proton contamination. Although such events are rare, a few per solar cycle, the fluences can be very high and can only be treated as random anomalously large enhancements (ALEs). The consequences of CMEs are more difficult to track, but there is now good evidence that significant electron enhancements of the outer belt are sometimes produced.[18–20]

Traffic Light Days

The GOES data sets have been excellent for monitoring enhancements of penetrating electrons (>2 MeV) since 1987 and

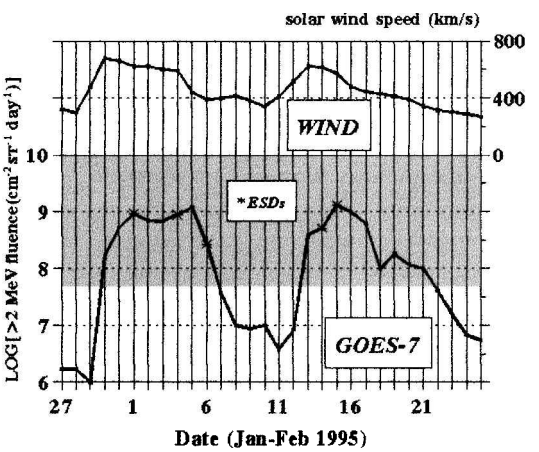

Fig. 1 Outer belt enhancements at GEO following increases in solar wind speed.

have proved ideal for establishing links with internal charging effects.[2] Comparisons with data from STRV-1 (discussed later) have indicated that these enhancements generally encompass the whole outer belt. Wrenn and Smith[21] have showed that a particular phantom command anomaly on a GEO platform requires a threshold 2-day fluence of 10^8 cm^{-2} sr^{-1}. Consequently daily fluences have been classified as low (green), high (amber), or extreme (red) based on thresholds at 5×10^7 and 5×10^8 cm^{-2} sr^{-1}. Figure 2 shows the GOES-7 data for 1993 in this format when ordered by CR; days lacking data due to contamination of the detector by protons with energy greater than 32 MeV remain white, and days on which their anomalies occurred are denoted by asterisks.

Register of Enhancements

It is now possible to define enhancements throughout the whole data set; the start being the first day that the daily fluence exceeds 5×10^7 cm^{-2} sr^{-1} and the duration given by the number of days it remains above this level, the sum of red and amber days; the 1993 extract from the full listing is presented as Table 1.

Total fluence is the sum for the enhanced days, and the rotation day is that of maximum fluence. The listing supplies the numerical detail of Fig. 2. Table 2 summarizes the distribution of the enhancements over the 11 years, showing the trend with smoothed sunspot number; values for 1986 and the first half of 1987 are from GOES-5 and may be artificially high due to detector noise.

During the 11-year period 184 enhancements were identified, with a mean duration of 6.9 days. Of the 4018 days, 1216 (30%) were enhanced (amber) and 275 (7%) were extremely enhanced (red).

Seasonal Variation

Seasonal structure is highlighted in Fig. 3 by plotting, on a logarithmic scale, all amber and red GOES >2-MeV daily fluences against fraction of year counted from a winter solstice.

The maximum envelope has peaks at equinox and troughs at solstice with year end significantly lower than midyear. This pattern is common to various geomagnetic indices and seems to reflect a more efficient coupling between the solar wind and the magnetosphere near equinox.

Table 1 Outer belt enhancements during 1993[a]

Code	Start date, 1993	No. red, day	No. amber, day	Maximum fluence/cm^2 · sr	Total fluence × 10^8	Rotation day (0–27)	CR
93a	3 Jan.	0	8	2.7*E*+08	14.2	14	1864
93b	1 Feb.	0	6	2.3*E*+08	8.1	13	1865
93c	8 Feb.	0	9	2.3*E*+08	12.4	20	1865
93d	22 Feb.	0	6	3.2*E*+08	12.2	6	1866
93e	3 March	0	4	1.1*E*+08	3.3	16	1866
93f	12 March	1	8	6.2*E*+08	17.7	3	1867
93g	22 March	0	7	2.0*E*+08	8.2	7	1867
93h	6 April	0	6	3.6*E*+08	7.8	26	1867
93i	16 April	1	3	5.7*E*+08	8.8	4	1868
93j	21 April	0	8	1.9*E*+08	7.1	8	1868
93k	10 May	0	16	3.8*E*+08	24.1	2	1869
93l	5 June	5	1	1.6*E*+09	65.4	3	1870
93m	14 June	0	3	5.0*E*+07	1.3	10	1870
93n	25 June	0	4	1.1*E*+08	3.6	19	1870
93o	11 July	0	7	2.9*E*+08	11.4	11	1871
93p	22 July	0	5	1.8*E*+08	6.2	20	1871
93q	8 Aug.	0	5	1.8*E*+08	6.5	9	1872
93r	17 Aug.	6	3	2.1*E*+09	100.7	23	1872
93s	4 Sept.	5	3	1.2*E*+09	48.7	10	1873
93t	14 Sept.	6	1	1.9*E*+09	86.7	21	1873
93u	1 Oct.	0	5	3.6*E*+08	10.1	10	1874
93v	10 Oct.	3	5	1.1*E*+09	41.7	19	1874
93w	5 Nov.	6	3	9.3*E*+08	47.1	18	1875
93x	3 Dec.	0	5	3.0*E*+08	9.1	19	1876
93y	17 Dec.	0	7	3.0*E*+08	11.2	5	1877
93(25)	——	33	138	2.1*E*+09	573.6	——	——

[a]Mean duration, 6.8 day.

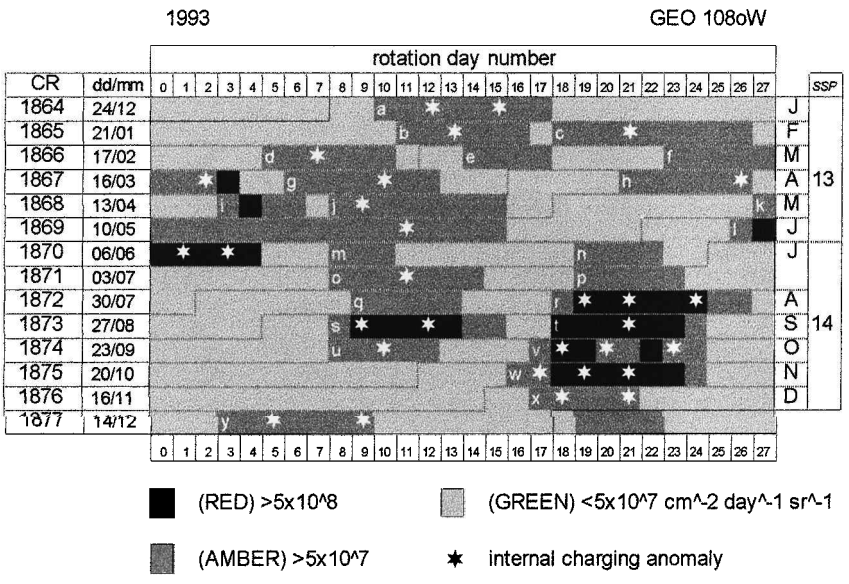

Fig. 2 Traffic light representation of GOES-7 daily fluence of >2-MeV electrons during 1993 with reported ESD anomalies.

Table 2 Outer belt enhancements, 1987–1998

Year	Number of events	Number of red, days	Number of amber, days	Number of amber + red	Mean duration, days	Total fluence, 10^8/cm^2 · sr	Smoothed sunspot no.[a]
1986	20	60	116	176	8.8	——	14
1987	12	6	58	64	6.0	103	32
1988	13	1	62	63	4.8	70	98
1989	8	0	48	48	5.5	55	154
1990	7	0	32	32	4.6	38	146
1991	12	4	55	59	4.9	85	144
1992	17	17	60	77	4.4	366	94
1993	25	32	139	171	6.8	573	56
1994	24	89	127	216	8.7	1275	30
1995	23	77	102	179	7.8	1312	17
1996	12	27	83	110	9.2	410	10
1997	16	11	79	90	5.6	205	23
1998	15	11	96	107	7.1	233	68
1987–1998	184	275	941	1216	6.9	4725	——

[a]Cycle 22 minimum in September 1986, maximum in July 1989, and minimum in May 1996.

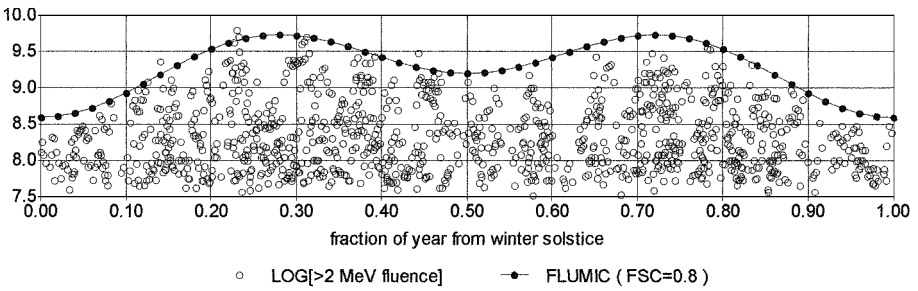

Fig. 3 Semi-annual variation of >2-MeV daily fluence in GEO during OBEEs since 1 July 1987; line is the FLUMIC model (L = 6.9) envelope.

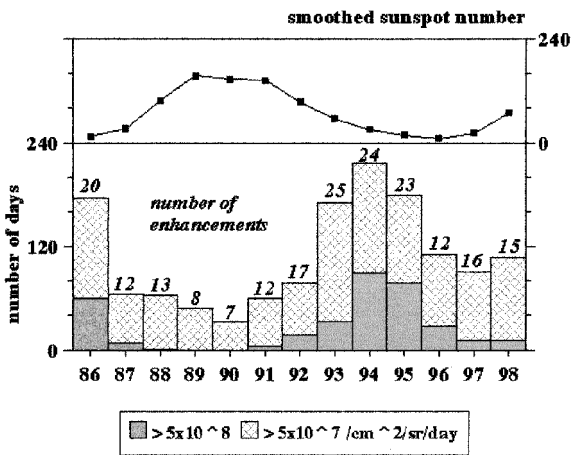

Fig. 4 Number of >2-MeV electron enhancements at GEO and number of red and amber days per year throughout the sunspot cycle.

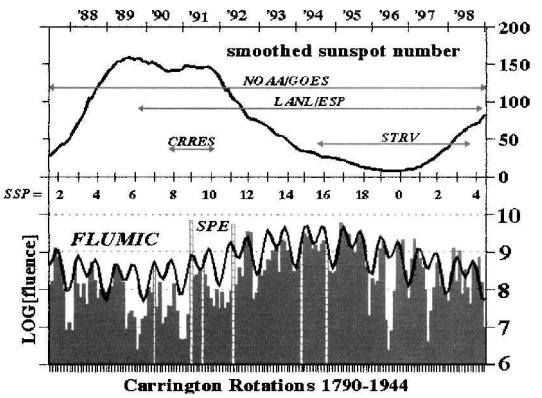

Fig. 5 Maximum daily fluence (cm^{-2} sr^{-1}) of >2-MeV electrons at GEO per CR throughout the sunspot cycle, six hatched bars are associated with SPEs; FLUMIC model for L = 6.9 plotted for comparison.

Solar Cycle Pattern

Baker et al.[22] conclude that "... the relativistic electron population in the outer magnetosphere undergoes the largest solar-cycle variation of any known particle population." This is based on data from GEO during cycle 21 when 27-day running averages of >1.4 MeV electrons ranged between 5×10^2 cm^{-2} s^{-1} sr^{-1} in 1979/1980 to 10^4 cm^{-2} s^{-1} sr^{-1} in 1984/1985. Yearly averages of >3-MeV electrons gave a factor of ~8 for the same epoch, whereas the amplitude variation of >0.43-MeV electrons was in-phase but smaller. The 1985 energy spectrum appears to be much harder than the 1980 spectrum.

The annual count of enhancements and overthreshold days in cycle 22, listed in Table 2 and plotted as Fig. 4, clearly supports the statement; the smoothed sunspot numbers for each year track the cycle from minimum in September 1986 through maximum in July 1989 to minimum in May 1996. Note how the enhancements peak during the declining phase of the cycle, just as they did in cycle 21. With internal charging, the frequency of days with fluence exceeding the appropriate threshold should determine the probability of discharge; the higher the threshold, the greater the role of the solar cycle seems to be. A more rigorous analysis was undertaken.

CR 1790 started on 16 June 1987 and CR 1944 started on 15 December 1998. Study of high resolution GOES-7 plots permitted many days to be coarsely classified in spite of some proton contamination. We determined the maximum fluence per rotation, and this is plotted in Fig. 5. Here six enhancements (23 March 1990, 27 March 1991, 10 July 1991, 11 May 1991, 21 February 1994, and 23 October 1994) are identified as being associated with SPEs; five more smaller ones (1 June 1990, 6 April 1991, 30 June 1992, 3 March 1993, and 21 October 1995) may be similarly linked. It is also possible that one or two onsets were obscured by extensive contamination during the active period in 1989.

The pattern set by Table 2 is plainly evident with the frequent recurrences covering a number of rotations and peak fluences during the second-half of the cycle being typically an order of magnitude higher than those during the first-half. The number of amber or red

days per rotation shows an even more marked bias toward the end of the declining phase. Increase in the frequency of enhancement events suggests that more fast solar wind streams reach the magnetosphere, whereas increase in event duration could reflect longer or stronger coupling with larger enhancements or reduced decay rates.

To facilitate the modeling, 20 sunspot phase (SSP) levels (SSP = 0–19), typically 7 rising plus 13 falling, have been specified to cover a cycle,[14] but cycles with a duration over 10 years require one or two extra segments to be appropriately rated. Because fluences tend to peak near equinox, it is logical to tie these levels to half-year segments centered at equinoxes. (January–June and July–December suffice.)

Energy Spectrum, Characteristic Energy, Hardness Coefficient

Because internal charge deposition critically depends on electron energy, it is important to establish the energy spectrum of the incident flux; an increase in integral flux F_E above a given energy E might result from general intensification, or a hardening of the spectrum or both. Baker et al.[22] contrasted GEO spectra for January 1980 and January 1985 to illustrate the existence of a significant solar cycle effect. Although the single-channel detector sensitive to >2-MeV electrons carried on GOES-7 offered no clues, a second channel sampling >0.6-MeV electrons was introduced on the later GOES satellites, and instruments with better energy discrimination have been flown on other missions. A complete empirical model ideally requires multipoint spectral measurements between 200 keV and 5 MeV covering the whole outer belt for at least a full solar cycle. Such measurements are not available, and given the uncertainties involved in the energy response calibrations and sampling integration, the assumption of a simple spectral function that can be inferred from a two-point spectrum offers the best compromise at present. Both exponential[2,22] and power law[14,23] distributions have been proposed, and here the former is selected, mainly because it offers better harmonization with the charge deposition calculations. In reality, the spectra are seldom exponential and never constant during the prolonged charging process.

By assuming that

$$F_E = F_0 \exp[-E/E_0] \tag{1}$$

the hardness of the spectrum is quantified by the characteristic e-folding energy E_0.

Given two integral fluxes, F_1 with energy greater than E_1 and F_2 with energy greater than E_2, then E_0 can be determined as

$$E_0 = (E_2 - E_1)\, \ell n[F_1/F_2] \tag{2}$$

In addition to invoking an exponential spectrum, this equation assumes that the detectors have sharp energy thresholds. If this is not the case, an equivalent measure of hardness can be determined from the count-rate ratio between two calibrated energy channels.[20] Either way it should be possible to obtain a first-order estimate for trends to be incorporated in the required model.

The solar cycle variation of energy spectrum has been explored using LANL ESP data for the period from 22 September 1989 to 22 October 1998. Daily averages of integral fluxes for electrons >1.8 MeV were analyzed to give a traffic light presentation, which was an excellent match for the GOES version when amber and red thresholds were set at 1.4×10^8 and 7.5×10^8 cm^{-2} sr^{-1} day^{-1}. Minor differences can be explained by the spacecraft spacings in longitude and local time.

For all days above the amber threshold, integral fluxes >0.7 and >3.5 MeV were also computed and Eq. (2) applied to estimate E_0. Figure 6 shows the resulting spread of values and their correlation with >1.8 MeV fluence. It supports the consistent finding that increasing flux of penetrating electrons generally corresponds with greater spectral hardness. Table 3 lists the maximum >1.8-MeV fluence and average E_0 for each 6-month SSP together with the numbers of days in each set; the fluence maxima and enhancement frequencies confirm the trend established earlier. Surveying all of the daily averages of E_0, there is a tendency to peak at SSP = 15, but the solar cycle dependence is not pronounced within the scatter, and it basically tracks the frequency of large fluence events. The spread of E_0 values about their mean is generally within ±20%, and this range needs to be incorporated into any worst-case model.

The CRRES mission proved less fruitful than hoped due to the premature end to operations after 14 months (see Fig. 5). The data set covers from 28 July 1990 to 10 October 1991, but the smoothed sunspot number was remarkably constant during this period, which featured only 12 enhancements from the GOES register; two of these followed SPEs including the only one to reach red levels, the truly amazing and probably unique March 1991 injection event. Vampola[14] attempted to extrapolate a solar cycle dependence utilizing a neural network relationship with ΣKp. Because he concluded[14] that a factor of only 2.6 should cover the variation of 140 keV to 1.54 MeV electrons over a cycle, it appears that his analysis was relatively insensitive to the critical enhancements of the hard component.

Table 3 Solar cycle variation of spectral hardness

				Enhancements	
Year	SSP	Data, days	Maximum fluence	days	E_0, MeV
1990/1	7	178	8.95E+08	31	0.46 ± 0.06
1990/2	8	183	5.01E+08	13	0.43 ± 0.06
1991/1	9	178	4.79E+09	34	0.50 ± 0.11
1991/2	10	184	7.61E+08	40	0.46 ± 0.04
1992/1	11	181	7.21E+09	26	0.47 ± 0.14
1992/2	12	184	5.00E+09	71	0.43 ± 0.08
1993/1	13	174	1.90E+09	95	0.46 ± 0.05
1993/2	14	182	2.29E+09	88	0.49 ± 0.08
1994/1	15	176	2.50E+09	127	0.54 ± 0.11
1994/2	16	180	2.07E+09	90	0.49 ± 0.08
1995/1	17	172	3.03E+09	89	0.50 ± 0.09
1995/2	18	153	1.26E+09	27	0.43 ± 0.07
1996/1	19	172	1.27E+09	33	0.40 ± 0.08
1996/2	0	176	1.53E+09	42	0.41 ± 0.08
1997/1	1	172	1.14E+09	36	0.40 ± 0.08
1997/2	2	184	5.38E+08	16	0.38 ± 0.09
1998/1	3	158	1.05E+09	22	0.42 ± 0.07

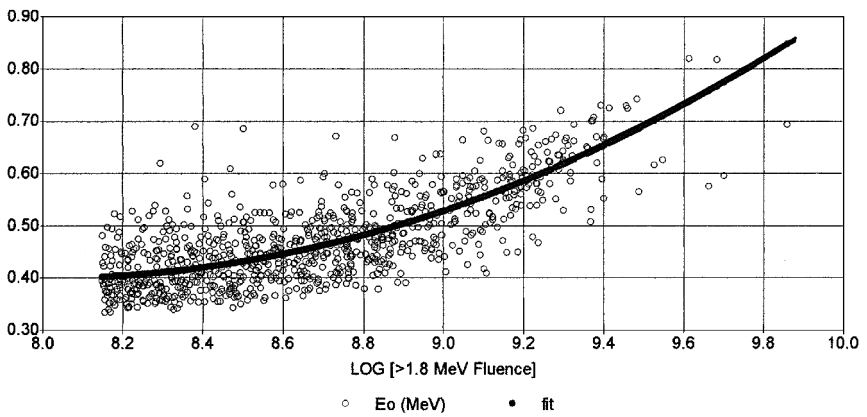

Fig. 6 Scatter plot of spectral hardness against >1.8-MeV fluence in GEO during OBEEs between 22 September 1989 and 22 October 1998.

Radial Profile

Can the evolving picture at GEO be extrapolated to the rest of the outer belt? Although GEO locations are in no way special with respect to charged particle dynamics, the measurements are at the outer fringe of the electron population. Because the background count rate of the HIPPARCOS star mapper was found to be raised by 3-MeV electrons, enhancements between December 1990 and February 1993 could be qualitatively mapped in L value.[13] Although centred around $L = 4$ the outer belt electron fluxes are highly variable in both space and time; at first sight one gets the impression that some significant enhancements might not be reflected in measurements at GEO.

The processes controlling the acceleration with transient trapping and subsequent loss of the electrons are poorly understood; the so-called recirculation theory[15] addresses the evolution and timing of enhancements but as yet it offers no clues on how the intensification and energization rates vary as a function of L. Here the relevant question is as follows: For each value of L, what is the maximum flux that is likely to be encountered? The relative timing within an enhancement event is academic.

Using 1.55-MeV data from CRRES, Brautigam et al.[24] confirm the spatial structure of enhancements, note the wide variation in the radial position of their inner edge, quantitatively describe the radial profiles in terms of "profile flux" and "centroid L" parameters, and show that these were moderately correlated with the *Ap15* planetary index. However, the relevance of these findings is questionable, given that their chosen example of an intense outer zone on 8 August 1990 fails to even reach the amber threshold at GOES-7.

A satellite in LEO at high inclination rapidly samples a full range of L values but detects only the particles that reach it, not those that mirror at higher altitudes. SAMPEX at 520–675 km carries two telescopes sensitive to MeV electrons and has produced extensive pictures of outer belt dynamics, but it is difficult to infer equivalent daily equatorial fluences from these measurements.

STRV-1a and STRV-1b were launched into GTO on 17 June 1994. STRV-1b carries a radiation environment monitor (REM) that measures the energy deposit of electrons in two independent shielded solid-state detectors[15]; the energy thresholds are approximately 1.0 and 2.0 MeV. STRV-1a carries a cold ion detector with a background count rate that is also sensitive to high-energy electrons.[8]

Results from STRV REM

Orbit-average count-rate and hardness ratio measurements for August 1994–May 1998 have been binned in terms of the L-value ranges listed in Table 4. The count rates are approximately proportional to integral flux greater than 1 MeV; the hardness ratio is simply the count-rate ratio between the two channels but using the energy response calibrations E_0 for an assumed exponential spectrum is approximated by $0.4/\ln(\text{hardness ratio})$.[20]

Threshold levels were selected to specify green, amber, and red days to highlight electron enhancements; again the red thresholds were chosen to tag the top 10% of the measurements in each bin, and the amber thresholds were then set at $\frac{1}{10}$th of these. Traffic light maps with the same format as Fig. 2 were compared with the GOES equivalents and found to match very well for all but the lowest L-value range. The average values of E_0, determined for both amber and red days, are presented in Table 4 together with the appropriate numbers of data and standard deviations and the maximum count rates for each bin.

Peak fluxes clearly occur near $L = 4.5$, and mean E_0 steadily increases as L gets smaller. The standard deviations at low L are relatively large, rendering these data as questionable because proton contamination is likely. If the electrons are accelerated by radial diffusion and redistributed with little energy loss by crossfield diffusion,[22] some systematic hardening as a function of L value might be expected in line with these results.

In April 1995, a fast solar wind stream produced a period of outer belt enhancement. REM data have been analyzed in greater detail to give the maximum flux measured in bins of 0.1 in L for three MeV energy ranges: $1.0 < E < 1.9$, $1.9 < E < 2.5$, and $2.5 < E < 4.5$; these differential fluxes have been converted to an integral flux for $E > 1$ MeV and plotted as Fig. 7. It is emphasized that these points do not represent a profile of outer belt electrons because peak fluxes at different L values occur at different times during an enhancement event. Desorgher et al.[25] have shown that at lower L values, high flux levels appear later and decay slower, and also that there is a semi-annual effect in that electrons penetrate deeper into the magnetosphere near equinox than during summer or winter. A curve fitted to the points, therefore, serves as a reasonable worst-case description of L-value dependence.

The four years of STRV data have been examined using the half-year SSP intervals to track the phases of the sunspot cycle. For each 6-month period, maximum count rate and an average E_0 for both amber days and red days were determined for the five L-value bins. The preminimum peak is substantiated by the maximum count rates for phases SSP = 16, 17, and 18, and there is more evidence for hardening associated with extreme enhancements. In general, the results are consistent with the picture of the whole outer belt electron population experiencing a similar level of enhancement during any of these events, when viewed with a resolution of at least 1 day and without regard to the relative timings.

FLUMIC

It is a requirement of the engineering tool that a meaningful electron spectrum is supplied in response to any orbit specification. Given the complexity of magnetospheric structure, the lack of understanding of the processes involved, and the paucity of good measurements, this cannot be presently achieved with high accuracy. Maximum integral flux (or fluence) for energies greater than 1 or 2 MeV can reasonably be predicted, but the energy spectrum is critical to the internal charging interaction, and it is difficult to extrapolate the observed solar cycle and L-value dependencies.

The development of required scaling algorithms is best suited by the simple exponential function of Eq. (1) but the selection of a reference energy E_R leads to a more convenient expression:

$$F_E(E, \text{FSC}, \text{FYR}, L) = a(L) \cdot F_R(\text{FSC}, \text{FYR}) \times \exp\left(\frac{\{E_R - E\}}{\{b(L) \cdot E_0(\text{FSC})\}}\right) \text{m}^{-2}\,\text{s}^{-1}\,\text{sr}^{-1} \quad (3)$$

Table 4 Maximum count rate and mean E_0, as a function of L value

STRV/REM data Aug. 94–May 98	Range in L value				
	2.5–3.5	3.5–4.5	4.5–5.5	5.5–6.5	6.5–7.5
Maximum count rate, s^{-1}	7.1E+03	8.6E+04	1.2E+05	2.0E+04	6.7E+03
Amber threshold, s^{-1}	300	5,200	5,800	1,000	185
% Amber days	23	23	23	23	23
Number of amber data	614	625	595	606	548
Mean E_0 for amber, MeV	0.67	0.44	0.39	0.34	0.32
Standard deviation, MeV	0.15	0.06	0.04	0.03	0.04
Red threshold, s^{-1}	1,050	21,500	24,000	4,800	880
% Red days	10	10	10	10	10
Number of red data	249	257	246	258	239
Mean E_0 for red, MeV	0.52	0.46	0.45	0.39	0.36
Standard deviation, MeV	0.11	0.05	0.03	0.03	0.03

Table 5 Six most intense enhancements seen in GEO since 1987

		Integral flux, cm^{-2} day^{-1} sr^{-1}					
		GOES	LANL ESP			E_0, MeV	
Month	Dates	>2 MeV	>0.7 MeV	>1.8 MeV	>3.5 MeV	0.7–1.8	1.8–7.8
March 1991	28/29	6.6E+09	1.7E+10	4.4E+09	5.6E+08	0.82	0.82
May 1992	11/12/13	2.9E+09	2.6E+10	4.7E+09	3.6E+08	0.65	0.66
Sept. 1992	5/6/7/8	2.2E+09	1.9E+10	2.6E+09	1.3E+08	0.55	0.57
Oct. 1992	2/3	3.5E+09	2.9E+10	4.8E+09	2.5E+08	0.61	0.57
March 1995	15/16	5.6E+09	1.3E+10	2.2E+09	1.5E+08	0.61	0.63
April 1995	13/14/15	4.1E+09	1.4E+10	2.7E+09	2.7E+08	0.69	0.73

where fraction of year (FYR) is 0 at a winter solstice rising linearly to 1 at the next and fraction of solar cycle (FSC = SSP/20) is 0 at a solar minimum rising linearly to 1 at the next.

Having established and coarsely quantified a set of trends, the remaining task is to combine them into a model that can satisfy the engineering requirements. Normalizing the measurements from different instruments necessarily involves some subjective judgement, given the complexities of calibration. By the use of $E_R = 2$ MeV, the GOES data are, thus, adopted as an absolute reference, on which the trends deduced from analyses of ESP and REM data are hung.

The functions appearing in Eq. (3) are simulated by following equations:

$$\log[F_R] = (8.8 + 0.5\sin[2\pi(\mathrm{FSC} - 0.55)]) \times (1 - 0.0435\cos[4\pi\mathrm{FYR}] - 0.0326\cos[2\pi\mathrm{FYR}]) \quad (4)$$

$$a(L) = 42(L - 2.8)^2 \exp[-0.39(L - 2.8)^2] \quad (5)$$

$$E_0 = 0.39 + 0.14\mathrm{FSC}, \quad \mathrm{FSC} \le 0.8$$
$$= 0.39 + 0.56(1 - \mathrm{FSC}), \quad \mathrm{FSC} > 0.8 \quad (6)$$

$$b(L) = 1.73 - 0.106L \quad (7)$$

Note that $a(L)$ and $b(L)$ are scaled to be unity for GEO, $L = 6.9$.

Equations (4) and (5) yield an envelope of maximum flux, whereas Eqs. (6) and (7) give an average spectral hardness for enhanced conditions, with ±20% being a reasonable spread band. Because high >2-MeV flux tends to correspond with high E_0, the +20% bound is likely to be more representative of severe internal charging conditions, but softer spectra, which could be relatively more damaging for lightly shielded dielectrics, should not be ignored. However, it is acknowledged that the expedient assumption of an exponential spectrum will seldom be meaningful below 200 keV, whereas no attempt is made to model the plasmasheet population.

For only 1.8% of days (4% of amber and 14% of red days, mainly ALEs) do the GOES fluences exceed the values given by Eq. (4). Data and FLUMIC model output ($L = 6.9$ and $E = 2$) are compared in Fig. 5.

The L-value dependence reflected by Eqs. (5) and (7) is clearly compromised by the lack of available data. The principal features of the outer belt electrons, the flux peak near $L = 4.5$, and the prevailing spectral hardening with decreasing L are roughly modeled, but with no temporal supplement. The flux peak position and perhaps its width could be described as functions of FYR and FSC if a more comprehensive set of reliable measurements were available.

FLUMIC fluxes for appropriate input variables are plotted in Figs. 3, 6, and 7 to illustrate the various dependencies.

Because the data sources used in the FLUMIC model do not provide off-equatorial measurements, the flux attenuation as a consequence of field-line displacement from the magnetic equator is introduced using expressions adopted in AE-4 (Ref. 26) and AE-8 (Ref. 4).

FLUMIC can be accessed as part of the DICTAT tool, which is available within the space environment information system (SPENVIS), on the Web at http://www.spenvis.oma.be [cited 12 May 2000].

Anomalously Large Enhancements

Since 1987, the six most enhanced events are those listed in Table 5. Daily averages of integral fluxes are shown for both GOES-7 and ESP detectors; with the latter, e-folding energies are calculated for 0.7–1.8-MeV and 1.8–7.8-MeV energy bands. Given the satellite spacings in longitude and local time, there is good agreement between the GOES and ESP measurements. The near equality of each pair of E_0 values suggests that the exponential assumption is not unreasonable. The first two enhancements were associated with solar proton events, but the other four were triggered by the arrival of high-speed solar wind at times of optimum magnetospheric coupling. The events do exhibit a range of spectral hardness but, with the exception of the March 1991 event, which is recognized as being unique, E_0 is confined to 0.63 MeV ±13%.

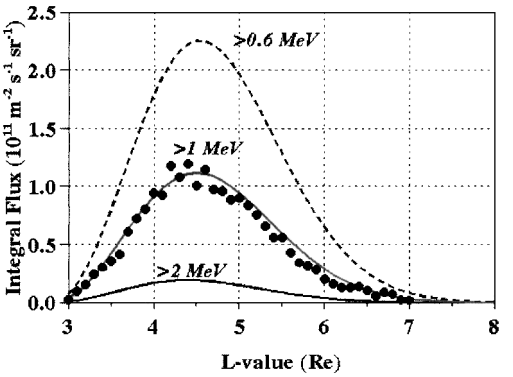

Fig. 7 Maximum flux (m^{-2} s^{-1} sr^{-1}) as a function of L value: >1-MeV data points from STRV/REM; >2-, >1-, and >0.6-MeV curves from FLUMIC model (FYR = 0.31 and FSC = 0.88).

As a supplement to the FLUMIC model an anomalously large enhancement can be treated by the substitution of the following two equations:

$$F_R[E_R = 2\,\mathrm{MeV}] = 6 \times 10^9\,\mathrm{cm}^{-2}\,\mathrm{day}^{-1}\,\mathrm{sr}^{-1} \quad (4a)$$

$$E_0 = 0.63 \pm 0.08\,\mathrm{MeV} \quad (6a)$$

A worst-case GEO spectrum is presented in a recent NASA technical handbook.[27] Because it is based on a single spectrum from measurements taken on 11 May 1992 over only a few hours at a selected longitude, it appears to be slightly harsher than that given here.

Discussion

FLUMIC is an empirical model that has been created for the specific application of internal dielectric charging of spacecraft in the magnetosphere. It has been generated from an appropriate but restricted data set. The critical solar cycle dependence has been largely deduced from routine monitoring in GEO during only one 11-year period, whereas the radial profile has been inferred from relatively few measurements in GTO. The model has been constructed with a built-in flexibility that provides scope for fine tuning. Its applicability could be enhanced by testing with other data, and any feedback of this kind would be most welcome. Of course the justification for a completely empirical model would diminish if a satisfactory theory of the electron acceleration mechanism could be established.[17]

Spacecraft should not contain unshielded dielectrics; when surface charging becomes relevant, the fluxes of electrons with energies

below 200 keV have to be considered, together with the complications introduced by secondary emission and photoemission. Effective modeling would then have to be fully time dependent with linkage to the local and transient nature of substorm processes in the magnetosphere.

The importance of peak fluences rather than average values has been stressed but there is always a dilemma in quantifying worst-case conditions: What should be done about the 100-year storm? Engineers have to decide what cost and risk tradeoffs are acceptable and what limits on contingency factors can be afforded. DICTAT users keen to develop bomb-proof systems have the option of inputting worst-worst-case spectra of their own choosing, but they must remember that such are not absolute but, rather, will be charge-site specific. Whereas shielding represents an ultimate form of protection, there are many other design rules and procedures that should be embraced to avoid problems caused by internal charging effects.[27]

Conclusion

FLUMIC has been designed to enable a prediction of the highest fluences of penetrating electrons to be expected during a mission; the orbit integrated fluences based on Eq. (3) should be considered as probable threat limits for normal operation. However, anomalously large enhancements do occur, and just a few per decade might cause problems. Rare soft errors in uncritical systems can usually be tolerated, but, for critical systems, the temporal functions of Eqs. (4) and (6) must be replaced by the higher levels that are specified by Eqs. (4a) and (6a). The model is presented as a significant advance on what was previously available, but it is hoped that further refinements can be included before the year 2004, when the internal charging hazard is due to peak again.

Acknowledgments

The work was supported by ESA technology research contracts under the Space Environments and Effects Major Axis, monitored by Eamonn Daly and John Sorensen (ESA Technical and Operational Support–Space Environments and Effects Analysis). The DERA part of these contracts was managed by Paul Latham. GOES data were supplied by NOAA Space Environment Laboratory; ESP data were supplied by Geoff Reeves of Los Alamos National Laboratory; METEOSAT-3 and STRV/cold iron detector data were supplied by the late Alan Johnstone of Mullard Space Science Laboratory, University College, London.

References

[1]Daughtridge, S., Garrett, H. B., and Whittlesey, A., "Environment-Induced Anomalies on the TDRS and the Role of Spacecraft Charging," *Journal of Spacecraft and Rockets*, Vol. 28, No. 3, 1991, pp. 324–329.

[2]Wrenn, G. L., "Conclusive Evidence for Internal Dielectric Charging Anomalies on Geosynchronous Communications Spacecraft," *Journal of Spacecraft and Rockets*, Vol. 32, No. 3, 1995, pp. 514–520.

[3]Rodgers, D. J., Ryden, K. A., Latham, P. M., Levy, L., and Panabiere, G., "Engineering Tools for Internal Charging: Final Report," ESA Contract 12115/96/NL/JG(SC), Aug. 1998.

[4]Vette, J. I., "The AE-8 Trapped Electron Model Environment," National Space Science Data Center, Rept. 91-24, Greenbelt, MD, Nov. 1991.

[5]Vampola, A. L., "ESA Update of AE-8 Using CRRES Data and a Neural Network," *Radiation Belts: Models and Standards*, edited by J. F. Lemaire, D. Heynderickx, and D. N. Baker, Geophysical Monograph 97, American Geophysical Union, Washington, DC, 1996, pp. 297–303.

[6]Cayton, T. E., Belian, R. D., Gary, S. P., Fritz, T. A., and Baker, D. N., "Energetic Electron Components at Geosynchronous Orbit," *Geophysical Research Letters*, Vol. 16, No. 2, 1989, pp. 147–150.

[7]Tsyganenko, N. A., "Global Quantitative Models of the Geomagnetic Field in the Cislunar Magnetosphere for Different Disturbance Levels," *Planetary and Space Science*, Vol. 35, No. 11, 1987, pp. 1347–1358.

[8]Wrenn, G. L., and Sims, A. J., "Internal Charging in the Outer Zone and Operational Anomalies," *Radiation Belts: Models and Standards*, edited by J. F. Lemaire, D. Heynderickx, and D. N. Baker, Geophysical Monograph 97, American Geophysical Union, Washington, DC, 1996, pp. 275–278.

[9]Evans, J., and Gubby, R., "Ground Loop Attitude Control for the Anik E Satellites," *Space Weather*, edited by R. Pirjola and D. Boteler, special issue of *Journal of Atmospheric and Solar Terrestrial Physics* (to be published).

[10]Szita, S., "Variability of 40–300 keV Electrons at Geosynchronous Orbit," Ph.D. Dissertation, Mullard Space Science Lab., Univ. of London, London, April 1998.

[11]Katz, I., Parks, D. E., Mandell, M. J., Harvey, J. M., Wang, S. S., and Roche, J. C., "NASCAP: A Three-Dimensional Charging Analyser Program for Complex Spacecraft," *IEEE Transactions on Nuclear Science*, Vol. 24, No. 6, 1977, pp. 2276–2280.

[12]Meier, M. M., Belian, R. D., Cayton, T. E., Christensen, R. A., Garcia, B., Grace, K. M., Ingraham, J. C., and Reeves, G. D., "The Energy Spectrometer for Particles (ESP): Instrument Description and Orbital Performance," *Workshop on the Earth's Trapped Particle Environment*, edited by G. D. Reeves, American Inst. of Physics Press, New York, 1996, pp. 203–210.

[13]Daly, E. J., van Leeuwen, F., Evans, H. D. R., and Perryman, M. A. C., "Radiation-Belt and Transient Solar-Magnetospheric Effects on Hipparcos Radiation Background," *IEEE Transactions on Nuclear Science*, Vol. 41, No. 6, 1994, pp. 2376–2382.

[14]Vampola, A. L., "The ESA Outer Zone Electron Model Update," *Environment Modelling for Space-based Applications*, SP-392, ESA 1996, pp. 151–158.

[15]Buehler, P., Ljungfelt, S., Mchedlishvili, A., Schlumpf, N., Zehnder, A., Adams, L., Daly, E., and Nickson, R., "Radiation Environment Monitor," *Nuclear Instruments and Methods in Physics Research*, Vol. A368, No. 6, 1995, pp. 825–831.

[16]Nakamura, R., Baker, D. N., Blake, J. B., Kanekal, S., Kleckner, B., and Hovestadt, D., "Relativistic Electron Precipitation near the Outer Edge of the Radiation Belt," *Geophysical Research Letters*, Vol. 22, No. 9, 1995, pp. 1129–1132.

[17]Reeves, G. D., "Relativistic Electrons and Magnetic Storms 1992–1995," *Geophysical Research Letters*, Vol. 25, No. 11, 1998, pp. 1817–1820.

[18]Baker, D. N., Li, X., Turner, N., Allen, J. H., Bargatze, L. F., Blake, J. B., Sheldon, R. B., Spence, H. E., Belian, R. D., Reeves, G. D., Kanekal, S. G., Klecker, B., Lepping, R. P., Ogilvie, K., Mewaldt, R. A., Onsager, T., Singer, H. J., and Rostoker, G., "Recurrent Geomagnetic Storms and Relativistic Electron Enhancements in the Outer Magnetosphere: ISTP Coordinated Measurements," *Journal of Geophysical Research*, Vol. 102, No. A7, 1997, pp. 14141–14148.

[19]Reeves, G. D, Friedel, R. H. W., Belian, R. D., Meier, M. M., Henderson, M. G., Onsager, T., Singer, H. J., Baker, D. N., Li, X., and Blake, J. B., "The Relativistic Electron Response at Geosynchronous Orbit During the January 1997 Magnetic Storm," *Journal of Geophysical Research*, Vol. 103, No. A8, 1998, pp. 17559–17570.

[20]Buehler, P., Desorgher, L., Zehnder, A., Johnstone, A., Daly, E., and Adams, L., "The Outer Radiation Belt During the 10 January 1997 CME Event," *Geophysics Research Letters*, Vol. 25, No. 15, 1998, pp. 2983–2986.

[21]Wrenn, G. L., and Smith, R. J. K., "Probability Factors Governing ESD Effects in Geosynchronous Orbit," *IEEE Transactions on Nuclear Science*, Vol. 43, No. 6, 1996, pp. 2783–2789.

[22]Baker, D. N., Goldberg, R. A., Herraro, F. A., Blake, J. B., and Callis, L. B., "Satellite and Rocket Studies of Relativistic Electrons and Their Influence on the Middle Atmosphere," *Journal of Atmospheric and Terrestrial Physics*, Vol. 55, No. 13, 1993, pp. 1619–1628.

[23]Koons, H. C., Gorney, D. J., and Blake, J. B., "Long-Term Variability of Electron Radiation Dose in Geosynchronous Orbit," *Journal of Spacecraft and Rockets*, Vol. 31, No. 4, 1994, pp. 557–561.

[24]Brautigam, D. H., Gussenhoven, M. S., and Mullen, E. G., "Quasi-static Models of Outer Zone Electrons," *IEEE Transactions on Nuclear Science*, Vol. 39, No. 6, 1992, pp. 1797–1803.

[25]Desorgher, L., Buhler, P., Zehnder, A., Daly, E., and Adams, L., "Variations of the Outer Radiation Belt During the Last Two Years," *Environment Modelling for Space-based Applications*, SP-392, ESA, 1996, pp. 137–142.

[26]Singley, G. W., and Vette, J. I., "The AE-4 Model of the Outer Radiation Zone Electron Environment," National Space Science Data Center, Rept. 72-06, Greenbelt, MD, Aug. 1972.

[27]"Avoiding Problems Caused by Spacecraft On-Orbit Internal Charging Effects," NASA HDBK-4002, Feb. 1999.

A. C. Tribble
Associate Editor